IIETA International Information and Engineering Technology Association
Advancing the World of Information and Engineering

Mathematical Modelling of Engineering Problems
Vol. 12, No. 11, November, 2025, pp. 4027-4040
Journal homepage: http://iieta.org/journals/mmep

Determinant Parameters for Accurate Representation of Cyclic Response of Reinforced Concrete Beam-Column Joints: Numerical Model Calibration

Dinda Ainur Istiqomah[1], Stefanus Adi Kristiawan[1*], Senot Sangadji[1], Buntara Sthenly Gan[2]

[1] Department of Civil Engineering, Universitas Sebelas Maret, Surakarta 57126, Indonesia
[2] Department of Architecture, College of Engineering, Nihon University, Fukushima 963-8642, Japan

Corresponding Author Email: s.a.kristiawan@ft.uns.ac.id

https://doi.org/10.18280/mmep.121129

Received: 8 September 2025
Revised: 3 November 2025
Accepted: 12 November 2025
Available online: 30 November 2025

Keywords:
parameter sensitivity ranking, finite element modeling, bar with memory bond, boundary condition, unloading factor, mesh configuration effect

ABSTRACT

This study calibrates a finite element (FE) model for reinforced concrete beam-column joints (BCJ) under cyclic loading. The objective is to clarify which parameters most influence the accuracy of FE simulations. Instead of relying on qualitative or ad hoc adjustments, this work introduces a systematic sensitivity ranking tailored to the cyclic response of BCJ. The methodology systematically evaluated mesh configuration, boundary conditions, and properties of concrete and reinforcement. The analysis followed ATENA guidelines, code provisions, and the approach used in previous research. The results showed that boundary conditions had a direct impact on the distribution of forces, moments, and deformations. The concrete hysteretic parameters had the most significant influence on model performance, exceeding the effects of mesh density or secondary material assumptions. However, when analyzing crack propagation, a finer mesh size provided the most accurate outcome. This study concludes that the proposed sensitivity ranking establishes a robust framework for model calibration. It enables researchers and engineers to reduce modeling uncertainty and improve the predictive accuracy of nonlinear analyses for RC beam-column joints.

1. INTRODUCTION

The finite element modeling (FEM) is widely recognized as a robust technique for simulating structural behavior in both static and dynamic analyses, particularly when experimental testing is constrained by the extensive range of parameters and high associated costs [1-3]. Numerical modeling enables the detailed visualization of composite element behavior, including stress-strain distributions, crack initiation and propagation, and plasticity indices. Studies utilizing software platforms such as ATENA, ABAQUS, ANSYS, DYNA, and OpenSees have achieved varying levels of success in replicating hysteretic responses; however, discrepancies remain due to inconsistent calibration methodologies [1, 4-10]. Validation against full-scale laboratory specimens under controlled and identical conditions is essential for evaluating and refining numerical models until the desired accuracy is achieved [3]. Key parameters, including mesh density, concrete damage plasticity, and bond-slip behavior, significantly affect simulation outcomes, yet their relative sensitivities are not well quantified [4]. Furthermore, most studies examine these parameters individually, overlooking potential synergistic effects.

Guo et al. [11] conducted sensitivity analyses on mesh size and orientation by modeling fracture propagation in geometrically identical models with varying mesh sizes, demonstrating that coarse meshes can estimate peak load with an error of less than 8%. Purnomo et al. [12] employed ABAQUS to assess the sensitivity of boundary dimensions, mesh size, and additional parameters in statically loaded beams, though limitations in crack propagation visualization arose due to computational instability. Živaljić et al. [13] investigated the sensitivity of numerical parameters in the analysis of reinforced concrete structures using the FEM/DEM approach, emphasizing mesh refinement and penalty parameters to reduce numerical errors. Lowes et al. [14] emphasized model calibration and validation with ATENA software for simulating large reinforced concrete walls under flexural loading, employing a sensitivity method that minimizes mesh dependency and ensures solution convergence with mesh refinement.

In another study, Naeimi and Moustafa [15] investigated the behavior of UHPC bridge columns using FEM with DIANA and SAP 2000 software, focusing on the influence of various reinforcement and design parameters, although they did not explicitly present the sensitivity analysis steps. Setiawan [16] investigated efficient strategies for modeling punching failure in flat plates with sensitivity analysis on parameters such as mesh type and size, crack model, and compressive strength, while Indriyantho et al. [3] used a multi-criteria approach in the RBSM model to reduce the uncertainty of the main variables through load-displacement curve analysis on reinforced concrete beams with geopolymer haunches. From a methodological perspective, several studies use mesh optimization and constitutive model selection, but calibration is often unsystematic, partial, and reliant on trial-and-error.

Previous research has underscored the impact of mesh density, confinement effects, and concrete damage parameters. However, few investigations have systematically compared the sensitivity of these factors within a structured framework for cyclic loading. Moaveni et al. [17] further demonstrated, through ANOVA and meta-modeling, that simulation results are influenced not only by mesh dimensions but also by the uncertainty in identified modal parameters and the spatial density of measurement points.

Current modeling practices often rely on software defaults and code-based recommendations; however, variations in assumed material properties and simulation parameters can significantly impact the accuracy of results. For example, spatial variability in Young's modulus can induce localized stress concentrations, with a 20% variation resulting in a 15–25% earlier onset of plasticity under both tensile and compressive loads [18]. Despite this, limited attention has been paid to quantifying the influence of individual modeling parameters on overall simulation accuracy. Key factors, such as mesh type and size [19, 20], boundary conditions [21], critical compressive displacement [16], concrete tension stiffening [22, 23], and unloading factor [24], have been shown to significantly affect the cyclic response of reinforced concrete members. However, existing studies have not systematically ranked the sensitivities of these parameters, creating a gap in guidance for researchers and engineers seeking to optimize FEM approaches for reinforced concrete structures. Consequently, a unified and systematic sensitivity ranking is necessary to identify which model parameters most significantly influence the accuracy of FEM for beam-column joints subjected to cyclic loading.

In response, this current study introduces a systematic and repeatable framework for calibrating finite element models of reinforced concrete beam-column joints, focusing on a detailed parametric investigation of modeling assumptions for joints subjected to combined axial and cyclic lateral loads, as established by the experimental setup of Yang et al. [25]. The methodology employs a structured parametric sensitivity analysis encompassing mesh configuration, boundary conditions, and material properties of both concrete and reinforcement. Each parameter set is evaluated in accordance with ATENA guidelines, relevant code provisions, and established benchmark studies. The analysis produces a sensitivity ranking based on the model's hysteretic response and crack propagation patterns, which were generated from the accuracy model and the normalized mean square error (NMSE). The significance of this study is its focus on input parameters in the modeling process that were previously ignored, including the behavior of reinforcement under compression, concrete unloading factor, tension stiffening in concrete, and concrete critical compression displacement.

This study calibrates a finite element model for reinforced concrete beam-column joints under cyclic loading and determines the relative influence of key modeling parameters on simulation accuracy. By systematically varying key input parameters, the study assesses their impact on the accuracy of numerical predictions relative to experimental results. This approach reduces modeling uncertainty and improves the reliability of nonlinear cyclic simulations. The study identifies and ranks the sensitivity of simulation parameters, offering practical guidelines for prioritizing critical inputs in FEM of reinforced concrete structures. Ultimately, these findings aim to enhance the robustness and predictive capability of numerical tools for earthquake-resistant design and assessment of reinforced concrete infrastructure.

2. METHODS

The schematic of the methodology for each phase is illustrated in Figure 1. First, the authors have collected experimental data, including the test setup and the response. The aim ensured that assumptions regarding actual load conditions, specifications, and objectivity could be achieved concurrently. The FEM program was used to construct a model based on assumptions regarding geometry formation, mesh configuration, boundary conditions, load application, and material properties. The next stage involved sensitivity analysis of each input parameter assumption that affected model development and results. Finally, the output data of BCJ behavior (hysteresis response and crack patterns) is collected and validated against experimental results to obtain modeling results with a reasonable error.

2.1 Numerical model development

For details of the specimens and test setups in the experimental test, readers are referred to the research conducted by Yang et al. [25], as detailed in Figure 2. In this study, FEM simulations were performed using ATENA because it has been widely used for RC structure analysis, including joints [26-30]. To enable reliable and simple convergence at every load step, the solution parameters used the modified Newton-Raphson recurrent solution with the elastic predictor, and readers are referred to the ATENA theory [31].

The fracture-plastic model [32, 33] served as a basis for the nonlinear constitutive model of concrete (Cementitious2), which was employed in this investigation. The concrete behavior in compression under multiaxial stress circumstances is represented by the Men's-William plasticity failure model [31, 34]. The location of the surface failure is not fixed; it can change depending on the strain parameter [31]. Additionally, a nonlinear hardening and softening phase regulates the failure surface [27]. The softening phase of the compression model is determined by displacement, and the crush band approach is used to guarantee mesh objectivity [34, 35]. In contrast, the hardening phase is determined by strain in the local coordinate system after the crack orientation [31]. The crack band technique [36-38] is used to characterize the post-cracking response of concrete [34] when crack initiation is defined by the Rankine failure criterion in the fracture model. An exponential softening function was used to depict the tensile stress-strain relationship of concrete upon cracking [35], with the Hordijk model [39] relating the tensile stress to the fracture energy and crack opening displacement.

When a crack appears in the concrete, it also causes a crack to appear in the concrete's joint element and causes nonlinear deformation in the joint element of a reinforcing bar [40]. The reinforcing elements exhibit a multilinear stress-strain relationship with hardening in proportion to stress and strain [31]. For the reinforcing bars, the Menegotto-Pinto model [41] was employed since it takes Bauschinger's effect into account during the unloading and reloading processes. The mechanical model for deformed reinforcing bars at the reinforced concrete interface serves as the basis for the numerical model of the reinforcing bar joint element used after a concrete fracture [42]. Following the nonlinear bond-slip formulation in the Fib

Model Code 2010 [43], bond-slip formulation with the geometry type of bar with memory bond was also taken into consideration. This was followed by the creation of geometry and mesh, the application of boundary conditions and loads, and the integration of concrete and reinforcement material properties, including bond relationships.

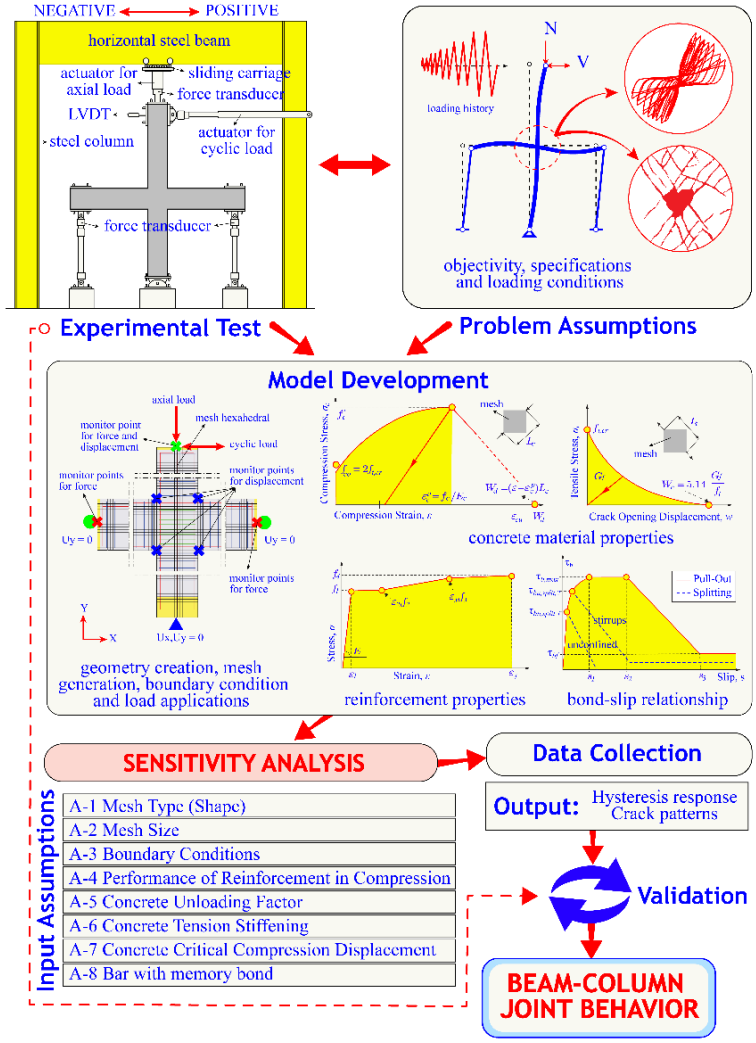

Figure 1. Systematic overview of FEM to evaluate beam-column joint behavior through sensitivity studies

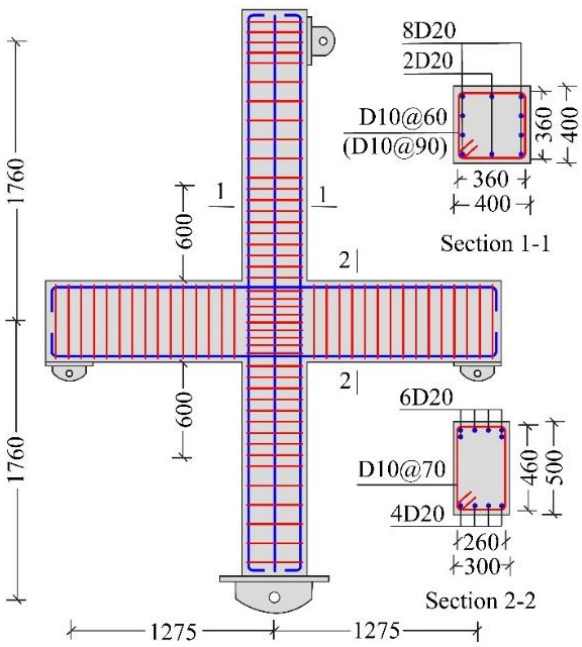

Figure 2. Test specimen details (unit: mm)

2.2 Quantitative sensitivity assessment

The sensitivity analysis method was generally divided into statistical (probabilistic) and numerical (deterministic) approaches. The statistical approach, often used in conjunction with Monte Carlo Simulation [44], required that well-defined probability distributions be established for the input parameters so that uncertainty in the inputs could be propagated to the outputs through repeated random sampling, with output results being expressed as probability distributions as well. However, in this study, such an approach could not be taken because the underlying parameter distributions were unknown and the available data were insufficient to define them accurately. Consequently, a numerical or deterministic approach was adopted, entailing an investigation of the model's response by varying input parameters.

The influence of each parameter on the model's predictive accuracy was assessed by calculating the NMSE [44, 45], which facilitated the identification of the most critical factors affecting the beam-column joint response. NMSE was used to quantitatively evaluate the predictive accuracy of the finite element model for each parameter variation. For each scenario, experimental results and numerical predictions were

obtained at every sampling point and normalized according to the following Eqs. (2) and (3). The NMSE was then computed using Eq. (1), where lower NMSE values indicate stronger agreement between the numerical model and experimental data.

$$NMSE = \frac{\sum_i s_i^2 (1 - k_i)^2}{\sum_i s_i k_i} \quad (1)$$

with

$$s_i = \frac{C_{oi}}{\bar{C}_o} \quad (2)$$

$$k_i = \frac{C_{pi}}{C_{oi}} \quad (3)$$

where, C_o and C_p are respectively observed (experimental) and predicted (numerical) concentrations, while the overbar indicates the mean over the sampling points, and i indicates the mean ith sampling point.

In addition, the accuracy percentage of the numerical output relative to the experimental output was calculated. The accuracy percentage provided an intuitive perspective on the extent to which the numerical results deviated from the experimental data. The accuracy percentage was determined by subtracting the error value, as shown in Eq. (4), from 100%. The error value was computed from the deviation ratio at each step (Eq. (5)). The accuracy percentage reflects the potential applicability of values for certain parameters. If the value obtained is close to 100%, the model is considered reliable in representing the experimental output.

$$Acc = 1 - e \text{ (in \%)} \quad (4)$$

with

$$e = \frac{\left(\sum_i \frac{C_{oi} - C_{pi}}{C_{oi}} \right)}{n} \quad (5)$$

where, A_{cc}: numerical accuracy percentage, e: numerical error percentage, and n: number of steps.

NMSE and accuracy percentage were used as complementary metrics to evaluate the sensitivity of the simulation model parameters. The combination of these two metrics enabled the identification of the most critical parameters through a ranking approach based on the magnitude of influence. In this context, the ranking process was initiated by converting the NMSE values into a 0–1 scale to facilitate comparison among parameters. Parameters with NMSE values lower than 0.1 and accuracy greater than 90% were classified as high-confidence and prioritized during calibration [46]. Parameters ranked at the top of the sensitivity analysis were required to undergo repeated experimental validation to minimize overfitting.

High sensitivity in a model is indicated when significant responses are produced due to variations in specific parameter values. Consequently, substantial errors can be introduced into the final results if these parameters are improperly calibrated. Therefore, parameters with the most significant sensitivity impact should be validated and tested with priority to ensure the accuracy and reliability of the structural analysis model. In addition, the study by Yu et al. [47] emphasized that calibration errors in high-sensitivity parameters could increase predictive deviation by up to 20%.

3. RESULTS AND DISCUSSIONS

3.1 Mesh type (Shape)

To evaluate the effect of using different types of solid mesh elements, two FE models were created, one with a structured mesh and another with an unstructured mesh. For both specimens, the mesh dimensions on the joint panel were made identical to facilitate observation of cracks in that area. In the case of unstructured meshes, the dimensions and shape of the elements on the joint panel were not controlled, as unstructured meshes are characterized by irregular element shapes and sizes, distinct from the consistent pattern of structured meshes. Figure 3 shows the surface crack pattern outcomes across different mesh types, while Figure 4 illustrates the envelope curve.

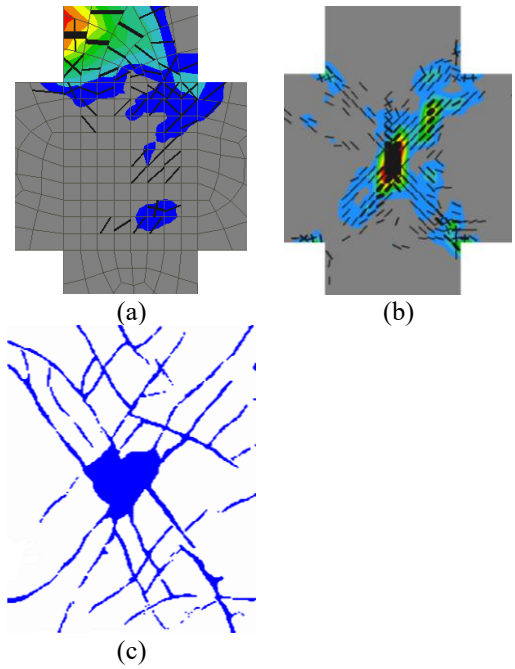

Figure 3. Crack patterns based on mesh type (shape)

Cracks were observed when the lateral force on the beam-column reached its peak. Visually, models with structured mesh tended to have crack patterns similar to those shown in the experimental results. In contrast, crack patterns in models with unstructured mesh showed cracks that were mostly located on the columns. The dominant failure location in unstructured mesh models, which shifts toward the column rather than the joint region, can be explained by fundamental principles: An inadequate mesh distorts the stress path, hinders the joint's ability to form a plastic hinge, and results in premature column failure. Tijssens et al. [48] have shown that the cohesive zone model exhibits a clear dependence on the crack pattern in the structured network, meaning that cracks tend to propagate along the dominant orientation of the elements. Therefore, in modeling cracks in rigid elements, unstructured meshes are recommended to reduce mesh dependence on crack patterns on a global scale. It should be

noted that, although from a global perspective mesh dependency can be reduced by using unstructured meshes, crack paths are still dependent on local mesh orientation, and it is necessary to prove that global crack patterns and critical loads are not affected by local mesh orientation when unstructured meshes are used.

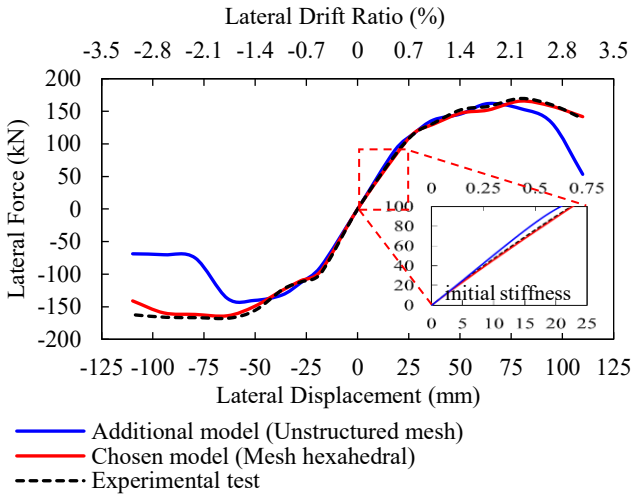

Figure 4. Load-displacement curve based on mesh type (shape)

In comparison to tetrahedral elements, hexahedral elements offer greater accuracy as they can better depict complex geometries, exhibit increased stability under various loading scenarios, and distribute stress more efficiently [49]. Tetrahedral elements typically exhibit a stiffer response than hexahedral elements at the same size [16], particularly when formed using non-uniform elements. The initial stiffness of the beam-column joint with an unstructured mesh is 10% greater than that of a joint with a structured hexahedral mesh. However, despite this increased initial stiffness, the joint with an unstructured mesh exhibits a significantly higher post-ultimate loss of stiffness, nearly 120% compared to its structured counterpart. This suggests that joints with an unstructured mesh are excessively stiff relative to expected conditions. On the other hand, the crack pattern observed in specimens with unstructured meshes indicates that failure is dominated by column elements. The failure mode suggests that the joint is unable to distribute deformation evenly, resulting in the column bearing more load than the joint itself. Consequently, this leads to flexural hinge failure in the column rather than an initial failure of the joint [50, 51].

It should be noted that in the numerical discretization of a continuous domain, the stress and strain around the fracture tip are only approximations. To approximate the stress gradient at the fracture tip as accurately as possible, the strategy is to use low-order elements for the entire domain and minimize the mesh size at the fracture tip. Another alternative is to use high-order elements. Further development can enrich the element library to improve accuracy without overloading the program.

3.2 Mesh size

A mesh dependency study was conducted to investigate the effect of mesh density on crack propagation. As the density of mesh elements increases, the integration points become closer to the stress concentration region, and the numerical solution converges to the exact solution. The computing resources required to run the simulation also increase as the mesh is refined. In this study, four mesh sizes of solid elements are simulated: 25 × 25 mm, 50 × 50 mm, 100 × 100 mm, and 200 × 200 mm. Following up further on the mesh shape that exhibits stability under various loading scenarios and stress distribution [49], the mesh shape used in the analysis is a 4-node hexahedral mesh. The reinforcement was modeled with a 1-D truss element, assuming a perfect bond between the elements. Crack propagation in four different finite elements and FEM representations in the same particle and matrix are shown in Table 1.

Table 1. Crack patterns based on mesh size

Mesh Size	Crack Patterns
200 × 200 mm (174 elements)	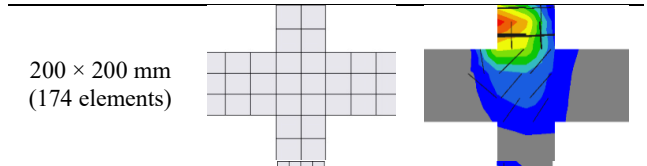
100 × 100 mm (402 elements)	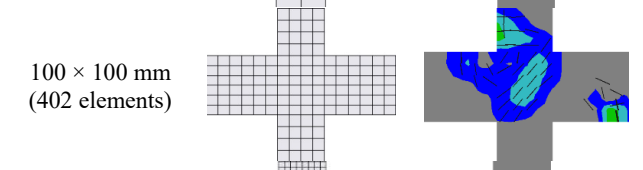
50 × 50 mm (1210 elements)	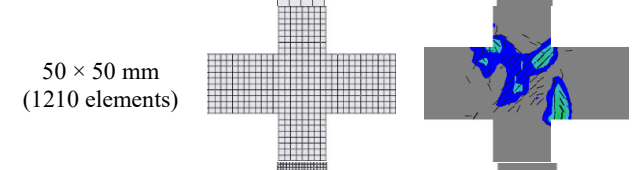
25 × 25 mm (4474 elements)	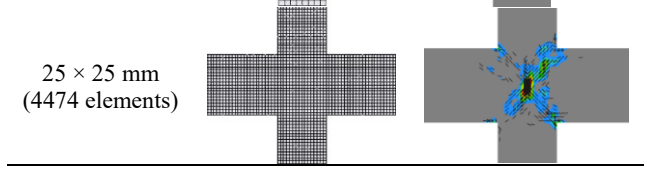

Finer mesh sizes, such as the 25 mm used in this study, are more accurate at capturing critical strains and accurately determining crack orientations compared to larger mesh sizes. This finding aligns with previous research indicating that finer meshes are reliable for detecting various types of cracks, including stress, diagonal shear, and compression cracks [52]. However, the use of finer meshes introduces smaller elements, which increases the number of degrees of freedom in the model. While this leads to a more detailed representation of the structure's geometry and behavior, it also necessitates longer computation times due to the increased number of equations that must be solved [53, 54].

When the element size is comparable to or exceeds the theoretical length of the plastic zone, the stress distribution surrounding the fracture tip approximates a uniform stress field. In this scenario, the overall stress exerts a greater influence on fracture propagation than the local stress field. In contrast, for fine meshes where the element size constitutes a small fraction, such as one-third, of the plastic zone length, the gradient of the local stress distribution within the plastic zone is accurately represented. Furthermore, if the mesh size is sufficiently small to represent the microstructure (e.g., mineral grains and grain boundaries) of quasi-brittle materials, the surface roughness of fractures observed from the mesh can accurately represent the roughness characteristics of the fracture material [55].

Figure 5 presents the envelope curve of each beam-column joint with various mesh sizes. Envelope curves of specimens

with mesh sizes exceeding 25 mm exhibit notable deviations from the anticipated curve. These specimens exhibit initial stiffness that is 5% to 15% slightly higher than those using fine meshes. Conversely, while coarser meshes may simplify the computational representation of the joint behavior, they can lead to less accurate predictions of peak load and stiffness degradation [19, 26, 56]. This occurs because the rate of energy release governing crack propagation becomes independent of the mesh when the mesh captures the essential stress concentration field.

Further development can enrich the elements to improve accuracy without burdening the program. Although computation time only increases in line with the number of elements, large-scale engineering problems may still require unrealistic computation time. Therefore, parallelization and the use of efficient algorithms for uncracked domains are necessary as solutions to computational constraints.

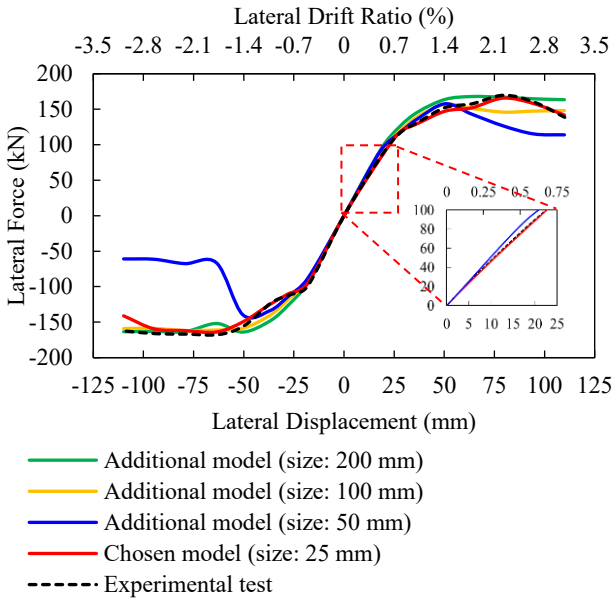

Figure 5. Load-displacement curve based on mesh size

3.3 Boundary conditions

To ensure the accuracy of the results, multiple sets of boundary conditions were examined in this study, as summarized in Table 2 and Figure 6.

BC-A is a joint with a constraint for point-pinned support $(u_x, u_y = 0)$ at the bottom of the column, and a constraint for point-roller support at both ends of the beam $(u_x = 0)$ (chosen model). BC-B is a joint with a constraint for line-pinned support at the bottom of the column $(u_x, u_y = 0)$, and a constraint for point-roller support at both ends of the beam $(u_x = 0)$. BC-C is a joint with a constraint for point-pinned support at the bottom of the column $(u_x, u_y = 0)$ and constraint for point-roller support $(u_x = 0)$ and the spring constraint at both ends of the beam. BC-D is a joint with a constraint for point-pinned support at the bottom of the column $(u_x, u_y = 0)$, constraint for point-roller support at both ends $(u_x = 0)$ and constraint for line-rotation support at the top end of the column $(r_z = 0)$.

Providing boundary conditions that presume rotational or movement constraints is crucial to accurately depicting how a beam-column joint will behave under this kind of pressure. In ATENA, various types of boundary conditions can be selected and tailored to meet the specific needs of the analysis. These boundary conditions significantly influence stress distribution, failure modes, and overall structural behavior.

Table 2. Combination of boundary conditions

Boundary Conditions	Crack Patterns
Experimental	
BC-A	
BC-B	
BC-C	
BC-D	

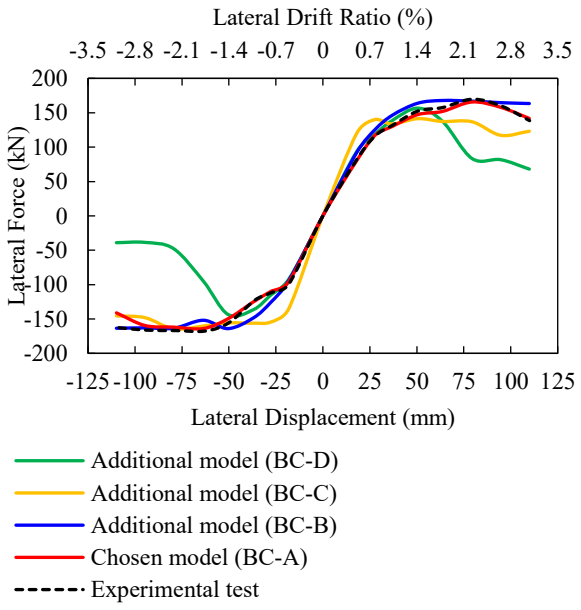

Figure 6. Load-displacement curve based on boundary condition combination

In specimen BC-A, diagonal cracks connect the corner joint, with the most substantial cracks appearing in the core joint. The diagonal crack connecting the corner joint in specimen BC-A is consistent with the shear failure mechanism commonly observed in beam-column joints under seismic loading [57]. This pattern indicates stress concentration at the core of the joint, consistent with the point-pinned support conditions that create local moment transfer. Conversely, specimens BC-B and BC-C exhibit cracks primarily in the column area near the joint, showing a shift in load distribution due to modified boundary conditions. Line-bound support at BC-B creates a more even stress distribution along the base of the column, altering the typical strong-column-weak-beam behavior. These line restraints artificially restrict lateral movement along the base width of the column, resulting in a more rigid response that resembles a pinched condition. This constraint increases stiffness beyond what is observed experimentally and causes cracks to localize primarily in columns adjacent to the joints. Such excessive constraint inhibits the expected softening and stiffness degradation that occur when steel reaches its yield point.

Similarly, spring constraints at BC-C introduce additional flexibility that redistributes stress away from the joint core [58]. These springs add extra stiffness at the beam-column interface, particularly noticeable at small drifts where spring force contributes to joint stiffness. The model thus overestimates initial stiffness by about 13% compared to experimental and BC-A data, and the spring forces reduce joint load capacity at higher drift levels by amplifying load on the column end. This artificial stiffness and resultant load redistribution cause discrepancies with expected failure and stiffness degradation. The force from displacement at the column's end grows with drift by amplifying spring strain, which reduces the joint load capacity [59].

Specimen BC-D exhibits a crack pattern similar to that of BC-A. The presence of additional rotation constraints on BC-D suggests that the roller support at the beam end primarily governs the joint behavior. In contrast, the larger cracks observed in the core and corners of BC-D imply that the line rotation support at the top of the column introduces secondary moment effects. This finding contradicts certain experimental results and underscores potential limitations in the current modeling of rotation constraints.

3.4 Performance of reinforcement in compression

In ATENA, users are given the option to disable reinforcement compression response. Not activating this menu means that steel bars resist tensile forces but do not contribute under compression. This is often used in simplified models or when compression yielding is unlikely (e.g., in beams with asymmetric reinforcement). Meanwhile, disabling this feature allows reinforcement to develop both tensile and compressive stresses according to its constitutive law (usually elastic–plastic with kinematic or isotropic hardening). Figure 7 illustrates the impact of activating this feature on the response of the beam-column joint structure subjected to cyclic loading.

Models including compression show pronounced pinching and reduced loop area for many beam/column configurations because crack opening/closing and concrete softening in compression reduce restoring forces on reversal [60]. When cracks reopen, the recovery of tensile stiffness is limited. In contrast, local compression and confinement degradation of concrete reduce the effective stiffness and energy absorption capacity in compression. As a result, the hysteresis loop narrows and bends. This reflects decreased cyclic energy dissipation and increased stiffness degradation. Such behavior is characteristic of the realistic response of reinforced concrete under cyclic loading. Here, tensile cracks and compressive damage develop path-dependently, resulting in asymmetric and bent hysteresis behavior.

Figure 8 illustrates that activating the compressive capacity of reinforcing steel reduces cracking in the joint cross-section compared to scenarios where its compressive contribution is not engaged. Considering compression behavior requires accounting for bond degradation and slip between concrete and reinforcing steel in both loading directions. These interactions influence load transfer, crack propagation, and stiffness degradation, which are essential factors for accurate simulation under cyclic loading. However, ignoring compression behavior ignores this instability mode, potentially leading to overestimation of load capacity and underestimation of damage accumulation.

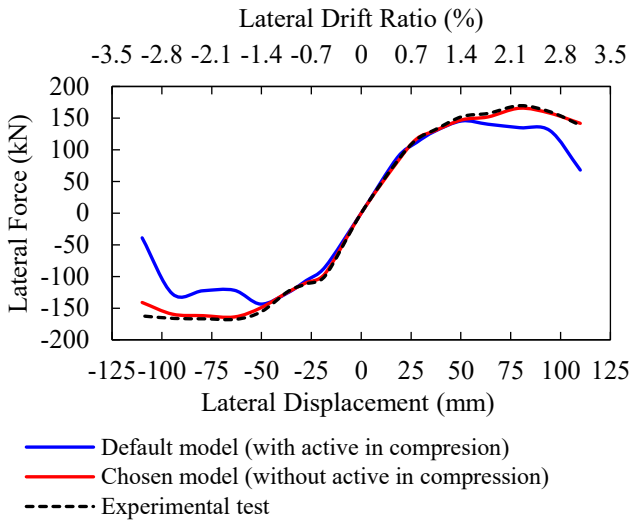

Figure 7. Load-displacement curve based on the performance of reinforcement in compression

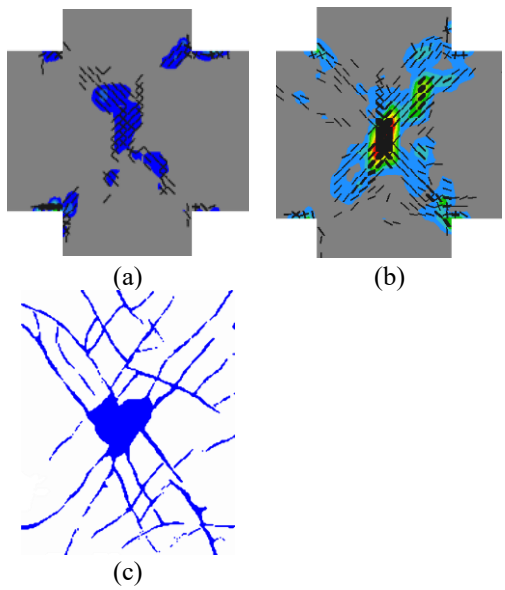

Figure 8. Crack patterns based on the performance of reinforcement in compression (a) with active in compression; (b) without active in compression; and (c) experimental

3.5 Concrete unloading factor

A high unloading factor (about 0.9) suggests that the model expects concrete to recover nearly all its stiffness upon crack closure. This presumes a full return to the original stiffness, which is unrealistic, as lasting microscopic damage, such as microcracking, aggregate slip, and adhesion loss, usually occurs. As a result, concrete does not restore its initial stiffness. Essentially, the model behaves more like an undamaged elastic material than a partially degraded one. In contrast, a low unloading factor (approximately 0.2) implies that concrete regains only a small fraction of its stiffness after cracks close. This is more accurate for alternating loads, since even when cracks close, imperfect contact, surface friction, and loss of aggregate interlock remain [32]. This mechanism limits stiffness recovery during loading, precisely emulating the clamping effect and the distinct reduction in stiffness observed in reverse cyclic loading. The resulting hysteresis loop is narrower and more asymmetric, reflecting authentic degradation in both stiffness and strength, and closely matching experimental observations.

The envelope curve of the concrete loading factor is illustrated in Figure 9 and Figure 10. The load-displacement curves show that the default model with an unloading coefficient of 0.9 substantially deviates from the experimental response, particularly in capturing the stiffness degradation and peak lateral resistance. A better approximation is achieved with an unloading coefficient of 0.5; however, the closest agreement with the experimental test is obtained when the unloading coefficient is reduced to 0.2, which successfully reproduces both the strength capacity and the post-peak softening behavior. Similarly, the crack patterns in Figure 10 further validate this finding. While higher unloading factors produce unrealistic crack distributions, the model with an unloading coefficient of 0.2 generates crack patterns that more closely resemble the experimental observations. These results indicate that careful calibration of the unloading factor is essential for improving the fidelity of FE models in simulating structural behavior under cyclic loading.

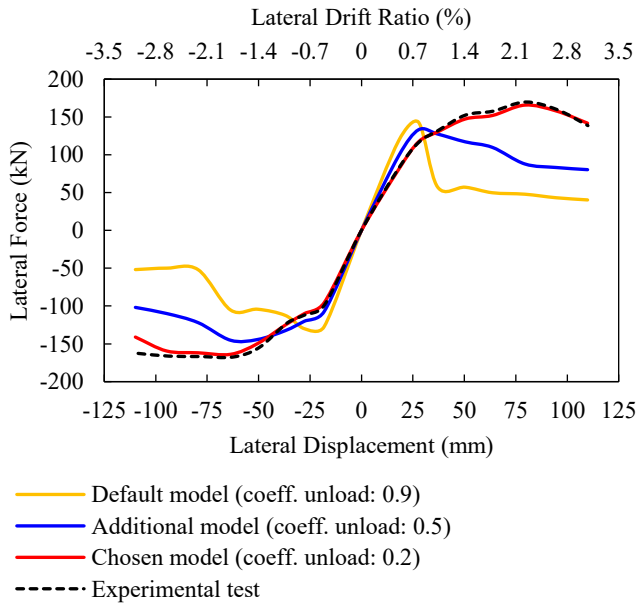

Figure 9. Load-displacement curve based on the concrete unloading factor

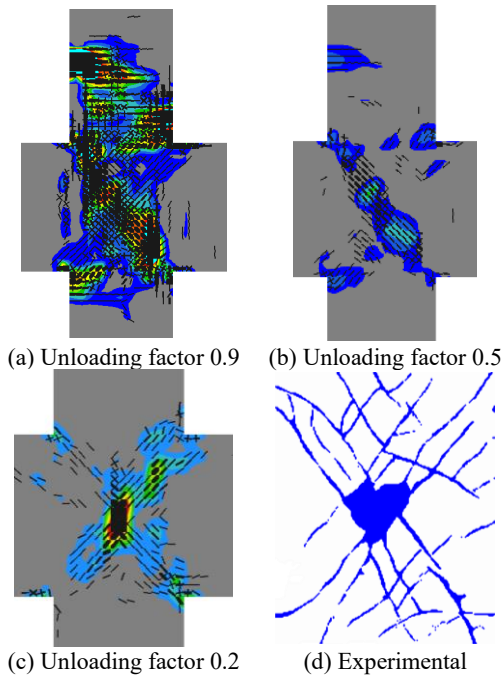

Figure 10. Crack patterns based on the concrete unloading factor

3.6 Concrete tension stiffening

Concrete tension stiffening refers to the phenomenon where concrete contributes to the overall tensile stiffness of reinforced concrete elements, even after cracking [61]. This effect arises from the bond between the concrete and the reinforcement, allowing some tensile stress to be transferred through the concrete between the cracks. Consequently, the structural elements increased stiffness due to the internal tensile forces absorbed by both the reinforcement and the uncracked concrete surrounding the cracks [62]. In ATENA, tension stiffening is an important factor in simulating the behavior of beam-column joints. This study presents several assumed values, illustrated in Figure 11 and Figure 12.

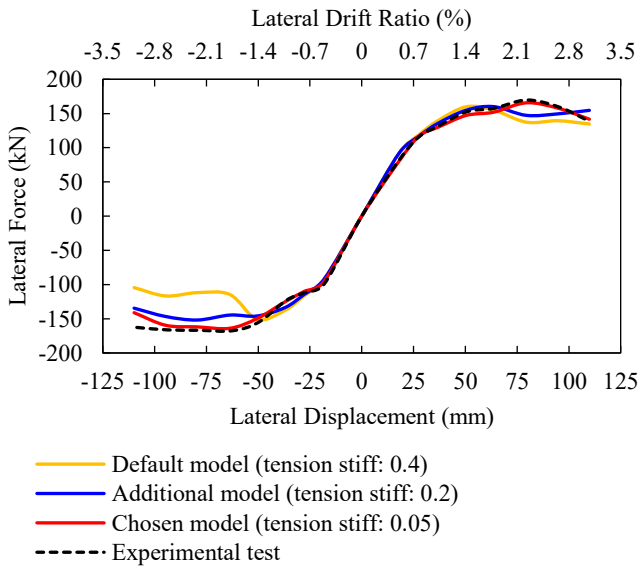

Figure 11. Load-displacement curve based on concrete tension stiffening

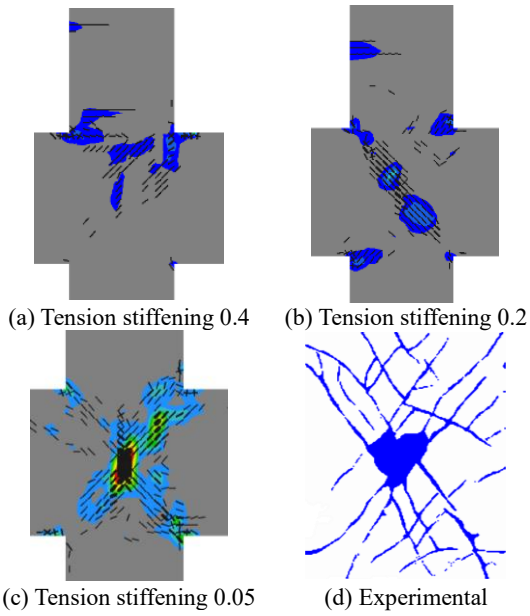

Figure 12. Crack pattern based on concrete tension stiffening

When the drift ratio approaches 3%, the predicted crack pattern diverges from experimental observations. High reinforcement stress values, such as 0.4, suggest that the model assumes concrete continues to carry most tensile stress after cracking. This assumption increases initial stiffness and delays crack formation, but also leads to overestimated load capacity and unrealistic crack patterns, as illustrated in Figure 12. In this scenario, the concrete-steel bond is modeled as excessively strong, thereby suppressing crack localization and obscuring the degradation effects typically observed in experiments. In contrast, lower tensile stiffness values decrease the joint's initial stiffness. A tensile stiffness value of 0.05 produces joint behavior that closely matches experimental results, particularly in terms of crack pattern distribution and the load-displacement response. Lower values indicate partial bond loss and reduced tensile stress transfer between shear cracks and microcracks at the steel-concrete interface. This leads to more localized cracking, a softer post-cracking response, and a hysteresis loop that aligns with experimental evidence [63].

3.7 Concrete critical compression displacement (W_d)

The parameter concrete critical compression displacement (W_d), governs the softening branch of the concrete compressive stress–strain relationship in numerical simulations. W_d defines the displacement at which the concrete stress in compression reduces to zero, representing the material's ductility in compression and the extent of post-peak softening. The research conducted by Setiawan [16] indicates that a higher value of W_d correlates with an increased capacity compared to other values. This correspondence produces a load-displacement curve that is similar to the experimental results, which is further supported by the distribution of crack patterns in the dynamic response (DR), which is close to 3%. Conversely, utilizing the default W_d leads to significant stiffness degradation before the specimen reaches its ultimate capacity.

The concrete softening curve in compression is modeled linearly in ATENA, with deformation expressed as displacement to ensure mesh objectivity [34, 35]. The standard value W_d was 0.5 mm. This scenario leads to premature stiffness degradation and underestimation of both ductility and energy dissipation. As a result, the numerical model demonstrates excessive brittleness and deviates from experimental results for load-displacement behavior and crack development. In contrast, higher values, such as 2.5 mm or 5 mm, allow the concrete to undergo greater inelastic deformation before complete softening. This modification increases the fracture energy absorbed during compression. The result is a smoother post-peak response and improved agreement with experimental data. Models with higher W_d more accurately reproduce both the peak load capacity and post-peak softening behavior seen in experiments.

The sensitivity of W_d was evaluated by simulating several values, including 2.5 mm and 5 mm. The corresponding results are shown in Figure 13 and Figure 14.

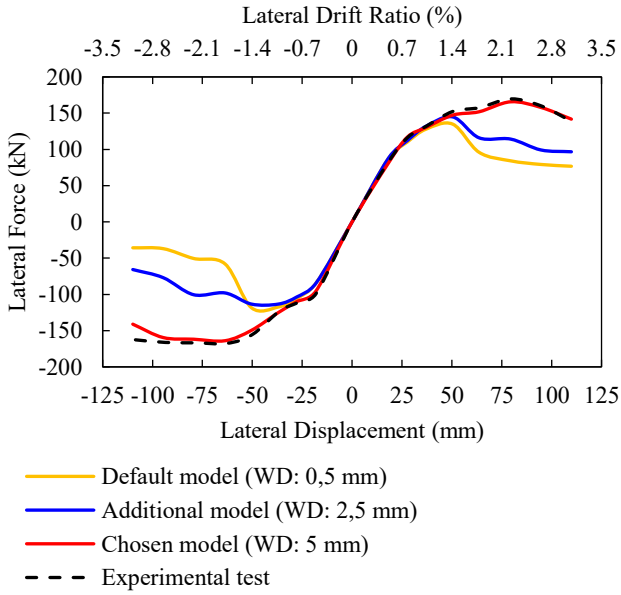

Figure 13. Load-displacement curve based on the concrete critical compression displacement

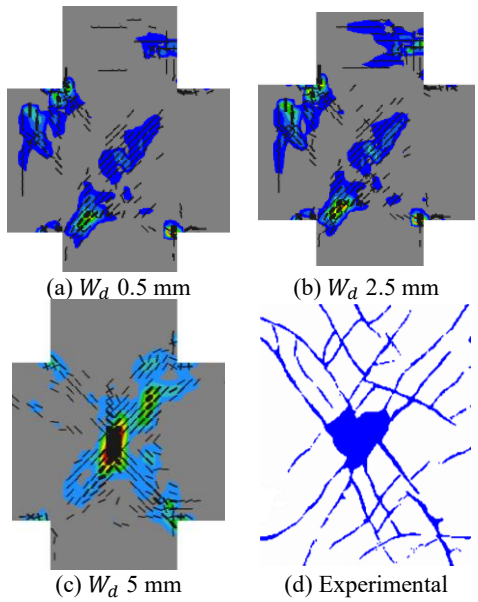

Figure 14. Crack patterns based on concrete critical compression displacement

3.8 Bar with memory bond

Reinforced concrete structures or elements involve concrete and reinforcement materials as their constituents. Therefore, the interaction between concrete and reinforcement is essential in analyzing the behavior of reinforced concrete structures, in this case, beam-column joints. In this study, two models were developed based on the involvement of input parameters in ATENA, steel-concrete bond slip, as shown in Figure 15 and Figure 16. The parameters used to define the bond between concrete and reinforcing steel are based on the Fib Model Code 2010 [43].

The application of bar memory bond explicitly accounts for shear behavior at the interface between reinforcing steel and concrete. This significantly influences the simulated response of RC structures under cyclic loading. Bar memory bond represents nonlinear interactions at the steel-concrete interface. Shear develops once the bond stress surpasses the interface's shear capacity.

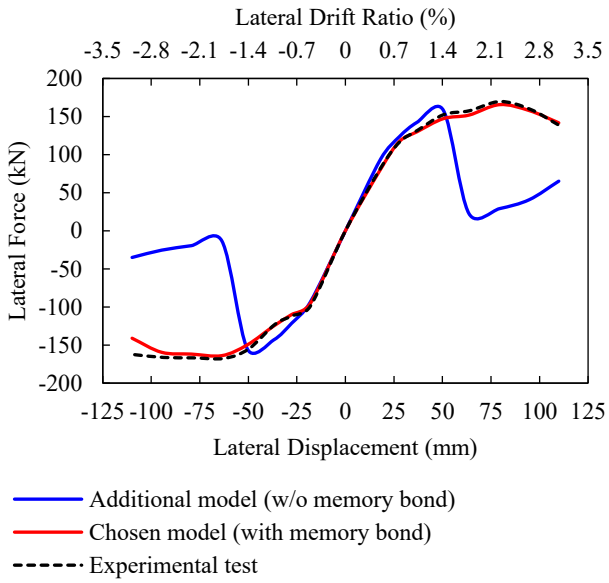

Figure 15. Load-displacement curve based on bar memory bond

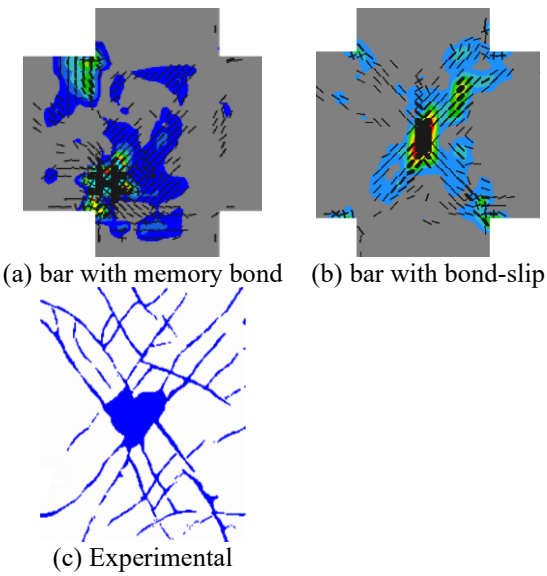

(a) bar with memory bond (b) bar with bond-slip

(c) Experimental

Figure 16. Crack patterns based on the bar memory bond

This behavior introduces hysteresis at the material level. It reflects the gradual degradation of adhesion and friction resulting from repeated load reversals. Models that neglect bond friction typically assume perfect bonding. These models require the reinforcing steel and concrete to deform identically. Such assumptions overestimate stiffness, strength, and energy dissipation. It disregards micro-friction, bond release, and re-anchorage of steel bars during cyclic loading.

As a result, simulated load-displacement curves are often unrealistically stiff, exhibiting limited compression and insufficient degradation in stiffness relative to experimental observations. In contrast, models that incorporate bond memory behavior capture progressive degradation at the steel-concrete interface. This produces more realistic compression, a reduced loop area, and accurate hysteresis degradation in the load-displacement response.

3.9 Parameter sensitivity ranking based on NMSE

Table 3 presents the results of accuracy and NMSE calculations for each input parameter. The ranking of the input parameter assumptions is visually represented in Figure 17.

Table 3. FE analysis versus experimental results based on the bar memory bond

ID	Parameter	Accuracy (%)	NMSE
A-1.1	Unstructured mesh	79.7451	0.1412
A-1.2	Mesh hexahedral	96.8926	0.0022
A-2.1	Mesh size: 200 × 200 mm	92.1464	0.0075
A-2.2	Mesh size: 100 × 100 mm	93.9427	0.0049
A-2.3	Mesh size: 50 × 50 mm	76.5521	0.1912
A-2.4	Mesh size: 25 × 25 mm	96.8926	0.0022
A-3.1	BC-A	96.8926	0.0022
A-3.2	BC-B	92.1464	0.0075
A-3.3	BC-C	82.8580	0.0330
A-3.4	BC-D	69.7842	0.3151
A-4.1	Reinforcement without active compression	96.8926	0.0022
A-4.2	Reinforcement with active compression	81.3116	0.1116
A-5.1	Concrete unloading factor: 0.9	49.9087	0.6216
A-5.2	Concrete unloading factor: 0.5	76.8460	0.1153
A-5.3	Concrete unloading factor: 0.2	96.8926	0.0022
A-6.1	Concrete tension stiffening: 0.4	86.3938	0.0479
A-6.2	Concrete tension stiffening: 0.2	92.2747	0.0099
A-6.3	Concrete tension stiffening: 0.05	96.8926	0.0022
A-7.1	W_d : 5 mm	96.8926	0.0022
A-7.2	W_d : 2.5 mm	75.5153	0.1661
A-7.3	W_d : 0.5 mm	65.6344	0.4133
A-8.1	Bar without memory bond	56.0315	0.7735
A-8.2	Bar with memory bond	96.8926	0.0022

Figure 17 illustrates the relationship between percentage changes in various input assumptions and corresponding changes in output accuracy, highlighting that each parameter exhibits a distinct level of sensitivity. Parameters such as A-3 (boundary conditions), A-4 (performance of reinforcement in compression), and A-8 (bar with memory bond) demonstrate the most significant impact on output, as indicated by their relatively large and positive gradients. Consequently, minor variations in these parameters can result in substantial fluctuations in the analysis or simulation results. Conversely, parameter A-2 (mesh size) has a data trend that tends to be flat, which indicates that changes in the value of this parameter do not affect the load achievement at each step.

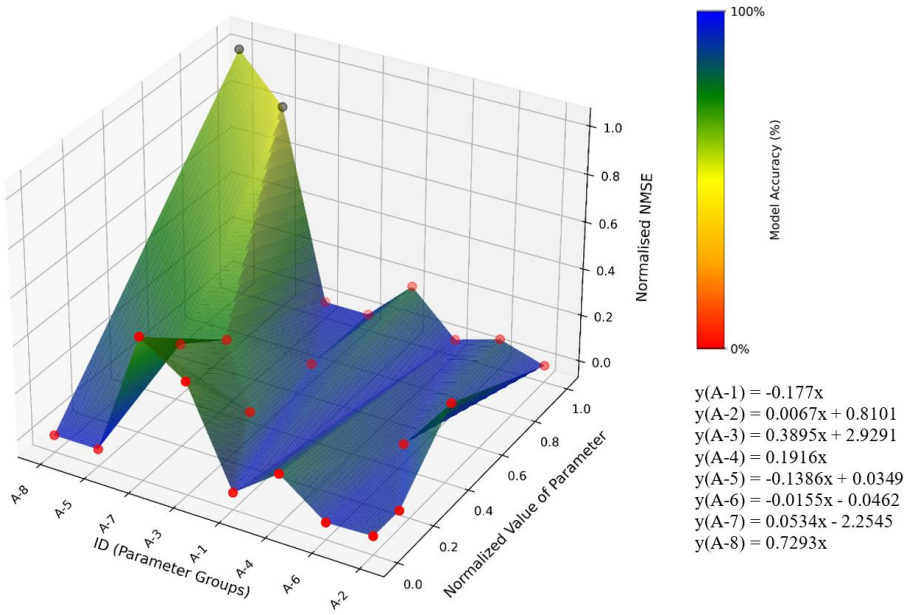

Figure 17. Parameter sensitivity ranking based on NMSE

4. CONCLUSIONS

Numerical simulations of beam-column joints in a 2D model were conducted to verify the model's accuracy with the expected results based on input parameters available in ATENA Science. Particular attention was given to the mesh configuration, boundary conditions, and the properties of concrete and reinforcement in predicting the response of beam-column joints under progressive cyclic loading. An analytical method was developed to identify and classify the most influential parameters affecting the modeling results, which are rarely considered, especially in cyclic behavior analysis. Furthermore, a sensitivity analysis was conducted to assess the impact of variations in each parameter on the structural response of the beam-column joints. Based on the presented results, the following conclusions were drawn:

1. An unstructured mesh is indeed preferred for crack simulations on quasi-brittle isotropic materials using a crack model. Before the actual simulation, the length of the theoretical plastic zone must first be estimated, then the element size is selected to be at least one-third of the length of the theoretical plastic zone as a network parameter or equal to the size of the element constituent grains.
2. Line support tends to distribute stress more evenly, preventing the local damage seen in point-supported specimens.
3. Ignoring the compressive capacity of steel for elements subjected to lateral loads is acceptable, but it needs to be evaluated in cases where the lateral load is in the form of beams, as this is related to pinching and energy dissipation effects.
4. Lower values of concrete tension stiffening indicate partial bond loss and reduced tensile stress transfer between shear cracks and microcracks at the steel-concrete interface.
5. Bars with memory bonds, reinforcement performance in compression, and boundary conditions must be given more attention in modeling than mesh configurations.

This study is limited to 2D numerical structures, which may not fully capture out-of-plane effects and complex stress interactions present in real 3D structures. The material and boundary assumptions used in the models were idealized and homogeneous, which may have led to deviations from experimental responses. Therefore, future work should consider incorporating 3D modeling, refined material characterization, and comprehensive experimental validation to enhance the reliability and general applicability of the numerical findings.

ACKNOWLEDGMENT

This work was supported by the Ministry of Higher Education, Science, and Technology for the PMDSU scholarship [Contract number: 1186.1/UN27.22/PT.01.03/2025].

REFERENCES

[1] Tamayo, J.L.P., Awruch, A.M., Morsch, I.B. (2013). Numerical modeling of reinforced concrete structures: static and dynamic analysis. Rem: Revista Escola de Minas, 66: 425-430. https://doi.org/10.1590/S0370-44672013000400004

[2] Landović, A., Čeh, A., Starčev-Ćurčin, A., Šešlija, M. (2024). Small-scale and large-scale modeling of fiber-reinforced concrete girders. Buildings, 14(12): 3812. https://doi.org/10.3390/BUILDINGS14123812

[3] Indriyantho, B.R., Purnomo, J., Purwanto, Ottele, M. Han, A.L., Gan, B.S. (2024). Multicriteria sensitivity analysis for numerical model validation of experimental data. International Journal of Technology, 15(6): 1644-1662. https://doi.org/10.14716/ijtech.v15i6.7146

[4] Ghorbanirenani, I., Tremblay, R., Léger, P., Leclerc, M. (2012). Shake table testing of slender RC shear walls subjected to eastern North America seismic ground motions. Journal of Structural Engineering, 138(12): 1515-1529. https://doi.org/10.1061/(ASCE)ST.1943-

541X.0000581
[5] Tambusay, A., Suryanto, B., Suprobo, P. (2020). Nonlinear finite element analysis of reinforced concrete beam-column joints under reversed cyclic loading. IOP Conference Series: Materials Science and Engineering, 930: 012055. https://doi.org/10.1088/1757-899X/930/1/012055
[6] Brünig, M., Michalski, A. (2020). Numerical analysis of damage and failure behavior of concrete. International Journal of Damage Mechanics, 29(4): 570-590. https://doi.org/10.1177/1056789519866005
[7] Al-Taai, A.A.S. (2025). Finite element analysis of concrete filled circular steel tube short columns subjected to axial compression load. Mathematical Modelling and Engineering Problems, 12(5): 1687-1694. https://doi.org/10.18280/mmep.120523
[8] Vidigal de Lima, M.C., El Debs, M.K. (2005). Numerical and experimental analysis of lateral stability in precast concrete beams. Magazine of Concrete Research, 57(10): 635-647. https://doi.org/10.1680/macr.2005.57.10.635
[9] Peng, Y.J., Wang, Q., Ying, L.P., Kamel, M.M.A., Peng, H.T. (2019). Numerical simulation of dynamic mechanical properties of concrete under uniaxial compression. Materials, 12(4): 643. https://doi.org/10.3390/ma12040643
[10] Pandimani, Ponnada, M.R., Geddada, Y. (2022). Numerical nonlinear modeling and simulations of high strength reinforced concrete beams using ANSYS. Journal of Building Pathology and Rehabilitation, 7: 22. https://doi.org/10.1007/s41024-021-00155-w
[11] Guo, L.W., Xiang, J.S., Latham, J.P., Izzuddin, B. (2016). A numerical investigation of mesh sensitivity for a new three-dimensional fracture model within the combined finite-discrete element method. Engineering Fracture Mechanics, 151: 70-91. https://doi.org/10.1016/j.engfracmech.2015.11.006
[12] Purnomo, J., Han, A., Gan, B.S., Hardjito, D. (2023). The effects of various parameters in sensitivity analysis of plain concrete beam using rigid body spring model. IOP Conference Series: Earth and Environmental Science, 1195: 012016. https://doi.org/10.1088/1755-1315/1195/1/012016
[13] Živaljić, N., Smoljanović, H., Nikolić, Ž. (2012). Sensitivity analysis of numerical parameters in FEM/DEM model for RC structures. International Journal for Engineering Modelling, 25(1-4): 7-17. https://hrcak.srce.hr/184949.
[14] Lowes, L.N., Lehman, D.E., Whitman, Z. (2019). Investigation of failure mechanisms and development of design recommendations for flexural reinforced concrete walls. Engineering Structures, 186: 323-335. https://doi.org/10.1016/j.engstruct.2019.01.122
[15] Naeimi, N., Moustafa, M.A. (2020). Numerical modeling and design sensitivity of structural and seismic behavior of UHPC bridge piers. Engineering Structures, 219: 110792. https://doi.org/10.1016/j.engstruct.2020.110792
[16] Setiawan, A. (2019). Efficient strategy for modelling punching failure of flat slabs. Doctoral dissertation, Imperial College of Science, Technology and Medicine, London. https://doi.org/10.25560/79982
[17] Moaveni, B., Conte, J.P., Hemez, F.M. (2009). Uncertainty and sensitivity analysis of damage identification results obtained using finite element model updating. Computer-Aided Civil and Infrastructure Engineering, 24(5): 320-334. https://doi.org/10.1111/j.1467-8667.2008.00589.x
[18] Song, Y., Schiffer, A., Tagarielli, V.L. (2021). The effects of heterogeneous mechanical properties on the response of a ductile material. Scientific Reports, 11: 1-17. https://doi.org/10.1038/s41598-021-97495-x
[19] Bracamonte, A.J., Mercado-Puche, V., Martínez-Arguelles, G., Pumarejo, L.F., Ortiz, A.R., Herazo, L.C.S. (2023). Effect of finite element method (FEM) mesh size on the estimation of concrete stress-strain parameters. Applied Sciences, 13(4): 2352. https://doi.org/10.3390/APP13042352
[20] Bakr, J., Ahmad, S.M., Lombardi, D. (2019). Finite-element study for seismic structural and global stability of cantilever-type retaining walls. International Journal of Geomechanics, 19(10): 04019117. https://doi.org/10.1061/(asce)gm.1943-5622.0001505
[21] Van Dorsselaer, N., Lapoujade, V., Nahas, G., Tarallo, F., Rambach, J.M. (2012). General approach for concrete modeling: Impact on reinforced concrete. In 12th International LS-DYNA® Users Conference, Dearborn. https://lsdyna.ansys.com/wp-content/uploads/attachments/blast-impact06-c.pdf.
[22] Morelli, F., Amico, C., Salvatore, W., Squeglia, N., Stacul, S. (2017). Influence of tension stiffening on the flexural stiffness of reinforced concrete circular sections. Materials, 10(6): 669. https://doi.org/10.3390/MA10060669
[23] Teng, L., Zhang, R.L., Khayat, K.H. (2022). Tension-stiffening effect consideration for modeling deflection of cracked reinforced UHPC beams. Sustainability, 14(1): 415. https://doi.org/10.3390/su14010415
[24] Khedmatgozar Dolati, S.S., Matamoros, A.., Ghannoum, W. (2024). Guidelines for Nonlinear finite element analysis of reinforced concrete columns with various types of degradation subjected to seismic loading. Infrastructures, 9(12): 227. https://doi.org/10.3390/INFRASTRUCTURES9120227
[25] Yang, H., Zhao, W.T., Zhu, Z.Z., Fu, J.P. (2018). Seismic behavior comparison of reinforced concrete interior beam-column joints based on different loading methods. Engineering Structures, 166: 31-45. https://doi.org/10.1016/j.engstruct.2018.03.022
[26] Maulana, H., Syaifa, L., Nabila, W.U., Thamrin, R., Kurniawan, R. (2023). Finite element model of reinforced concrete interior beam-column joints subjected to cyclic loading. E3S Web of Conferences, 464: 15007. https://doi.org/10.1051/e3sconf/202346415007
[27] Don, W., Suryanto, B., Tambusay, A., Suprobo, P. (2022). Forensic assessments of the influence of reinforcement detailing in reinforced concrete half-joints: A nonlinear finite element study. Structures, 38: 689-703. https://doi.org/10.1016/J.ISTRUC.2022.02.029
[28] Tambusay, A., Suryanto, B., Suprobo, P., Nelson, J.J.M. (2023). Nonlinear analysis of interior and exterior beam-column connections under reversed cyclic loading. IOP Conference Series: Earth and Environmental Science, 1195: 012018. https://doi.org/10.1088/1755-1315/1195/1/012018
[29] Purwanto, E., Adri, P.A., Kristiawan, S.A., Sangadji, S., Alfisa, S.H. (2022). Strengthening of non-engineered building beam-column joint to increase seismic

performance with variation of steel plate width. In Proceedings of the 5th International Conference on Rehabilitation and Maintenance in Civil Engineering, Surakarta, Indonesia, pp. 215-224. https://doi.org/10.1007/978-981-16-9348-9_19
[30] Haris, I., Roszevák, Z., Haris, I., Roszevák, Z. (2019). Finite element analysis of cast-in-situ RC frame corner joints under quasi-static and cyclic loading. Journal of Construction, 18(3): 579-594. https://doi.org/10.7764/RDLC.18.3.579
[31] Červenka, V., Jendele, L., Červenka, J. (2022). ATENA Program Documentation–Part 1 Theory. https://www.cervenka.cz/assets/files/atena-pdf/ATENA_Theory.pdf.
[32] Jefferson, A.D., Mihai, I.C. (2015). The simulation of crack opening-closing and aggregate interlock behaviour in finite element concrete models. International Journal for Numerical Methods in Engineering, 104(1): 48-78. https://doi.org/10.1002/nme.4934
[33] Cervenka, J., Cervenka, V., Eligehausen, R. (1998). Fracture-plastic material model for concrete, application to analysis of powder actuated anchors. In Proceedings of FRAMCOS-3, 3: 1107-1116.
[34] Červenka, J., Papanikolaou, V.K. (2008). Three dimensional combined fracture–plastic material model for concrete. International Journal of Plasticity, 24(12): 2192-2220. https://doi.org/10.1016/J.IJPLAS.2008.01.004
[35] Červenka, J., Červenka, V., Laserna, S. (2018). On crack band model in finite element analysis of concrete fracture in engineering practice. Engineering Fracture Mechanics, 197: 27-47. https://doi.org/10.1016/J.ENGFRACMECH.2018.04.010
[36] Bažant, Z.P., Oh, B.H. (1983). Crack band theory for fracture of concrete. Matériaux et Constructions, 16(3): 155-177. https://doi.org/10.1007/BF02486267
[37] Suryanto, B., Nagai, K., Maekawa, K. (2010). Smeared-crack modeling of R/ECC membranes incorporating an explicit shear transfer model. Journal of Advanced Concrete Technology, 8(3): 315-326. https://doi.org/10.3151/jact.8.315
[38] Don, W., Chong, K., Aitken, M., Tambusay, A., Suryanto, B., Suprobo, P. (2020). Influence of link spacing on concrete shear capacity: Experimental investigations and finite element studies. IOP Conference Series: Materials Science and Engineering, 930: 012052. https://doi.org/10.1088/1757-899X/930/1/012052
[39] Hordijk, D.A. (1992). Tensile and tensile fatigue behaviour of concrete; experiments, modelling and analyses. Heron, 37(1). http://worldcat.org/issn/00467316.
[40] Zivaljic, N., Nikolic, Z., Munjiza, A. (2011). A combined finite-discrete element model for reinforced concrete under seismic load. In COMPLAS XI: Proceedings of the XI International Conference on Computational Plasticity: Fundamentals and applications, pp. 788-795. https://congress2.cimne.com/complas2011/proceedings/full/p200.pdf.
[41] Menegotto, M., Pinto, P.E. (1973). Method of analysis for cyclic loaded RC plane frame including changes in geometry and non-elastic behaviour of elements under combined normal force and bending. In Proceedings of IABSE Symposium on Resistance and Ultimate Deformability of Structures Acted on by Well Defined Repeated Loads, pp. 15-22. http://doi.org/10.5169/seals-13741
[42] Soltani, M., Maekawa, K. (2008). Path-dependent mechanical model for deformed reinforcing bars at RC interface under coupled cyclic shear and pullout tension. Engineering Structures, 30(4): 1079-1091. http://doi.org/10.1016/J.ENGSTRUCT.2007.06.013
[43] Cairns, J. (2015). Bond and anchorage of embedded steel reinforcement in fib Model Code 2010. Structural Concrete, 16(1): 45-55. https://doi.org/10.1002/suco.201400043
[44] Garcia, D., Arostegui, I., Prellezo, R. (2019). Robust combination of the Morris and Sobol methods in complex multidimensional models. Environmental Modelling & Software, 122: 104517. http://doi.org/10.1016/J.ENVSOFT.2019.104517
[45] Poli, A.A., Cirillo, M.C. (1993). On the use of the normalized mean square error in evaluating dispersion model performance. Atmospheric Environment. Part A. General Topics, 27(15): 2427-2434. http://doi.org/10.1016/0960-1686(93)90410-Z
[46] Javadi, P., Askari, M.J., Vahedi, S., GhafourianHesami, A.H., Tizchang, A. (2023). Retrofit of RC buildings using vertical shear links and hybrid connections. Structures, 48: 1788-1807. http://doi.org/10.1016/J.ISTRUC.2023.01.015
[47] Yu, X., Robuschi, S., Fernandez, I., Lundgren, K. (2021). Numerical assessment of bond-slip relationships for naturally corroded plain reinforcement bars in concrete beams. Engineering Structures, 239: 112309. http://doi.org/10.1016/J.ENGSTRUCT.2021.112309
[48] Tijssens, M.G.A., Sluys, B.L.J., van der Giessen, E. (2000). Numerical simulation of quasi-brittle fracture using damaging cohesive surfaces. European Journal of Mechanics-A/Solids, 19(5): 761-779. http://doi.org/10.1016/S0997-7538(00)00190-X
[49] Schneider, T., Hu, Y., Gao, X., Dumas, J., Zorin, D., Panozzo, D. (2022). A large-scale comparison of tetrahedral and hexahedral elements for solving elliptic PDEs with the finite element method. ACM Transactions on Graphics (TOG), 41(3): 1-14. https://doi.org/10.1145/3508372
[50] Shu, J., Belletti, B., Muttoni, A., Scolari, M., Plos, M. (2017). Internal force distribution in RC slabs subjected to punching shear. Engineering Structures, 153: 766-781. https://doi.org/10.1016/j.engstruct.2017.10.005
[51] Hwang, H.J., Park, H.G. (2020). Plastic hinge model for performance-based design of beam-column joints. Journal of Structural Engineering, 147(2): 04020336. https://doi.org/10.1061/(ASCE)ST.1943-541X.0002892
[52] Zerfu, K., Ekaputri, J.J. (2021). Nonlinear finite element study on element size effects in alkali-activated fly ash based reinforced geopolymer concrete beam. Case Studies in Construction Materials, 15: e00765. https://doi.org/10.1016/J.CSCM.2021.E00765
[53] Nemade, A., Shikalgar, A. (2020). The mesh quality significance in finite element analysis. IOSR Journal of Mechanical and Civil Engineering (IOSR-JMCE), 17(2): 44-48. https://doi.org/10.9790/1684-1702054448
[54] Ismael, M.A., Abd, H.J., Abbas, S.R. (2023). Structural performance of reinforced concrete columns with bracing reinforcement. Annales de Chimie - Science des

Matériaux, 47: 287-296. https://doi.org/10.18280/acsm.470504
[55] Colpo, A.B., Kosteski, L.E., Iturrioz, I. (2017). The size effect in quasi-brittle materials: Experimental and numerical analysis. International Journal of Damage Mechanics, 26(3): 395-416. https://doi.org/10.1177/1056789516671776
[56] Mosallam, A., Allam, K., Salama, M. (2019). Analytical and numerical modeling of RC beam-column joints retrofitted with FRP laminates and hybrid composite connectors. Composite Structures, 214: 486-503. https://doi.org/10.1016/j.compstruct.2019.02.032
[57] Pasala, D.T.R., Sarlis, A.A., Nagarajaiah, S., Reinhorn, A.M., Constantinou, M.C., Taylor, D. (2013). Adaptive negative stiffness: New structural modification approach for seismic protection. Journal of Structural Engineering, 139: 1112-1123. https://doi.org/10.1061/(ASCE)ST.1943-541X.0000615
[58] Ehsani, M.R., Alameddine, F. (1991). Design recommendations for type 2 high-strength reinforced concrete connections. Structural Journal, 88(3): 277-291. https://doi.org/10.14359/3108
[59] Hosseini, M., Hosseini, H., Amin, S., Olounabadi, A., Hosseini, A. (2015). Study the effective of lateral load on story drift in RC frame structures. International Journal of Innovative Science and Modern Engineering (IJISME), 3(6): 32-43. https://www.ijisme.org/wp-content/uploads/papers/v3i6/F0861053615.pdf.
[60] Massone, L.M., Moroder, D. (2009). Buckling modeling of reinforcing bars with imperfections. Engineering Structures, 31(3): 758-767. https://doi.org/10.1016/J.ENGSTRUCT.2008.11.019
[61] Stramandinoli, R.S.B., La Rovere, H.L. (2008). An efficient tension-stiffening model for nonlinear analysis of reinforced concrete members. Engineering Structures, 30(7): 2069-2080. https://doi.org/10.1016/j.engstruct.2007.12.022
[62] Hernández Gil, L., Hernández Montes, E. (2023). Linear concrete tension stiffening model for reinforced concrete elements. Hormigón y Acero, 74(301). https://doi.org/10.33586/hya.2023.3097
[63] Wu, Z.S., Yoshikawa, H., Tanabe, T.A. (1991). Tension stiffness model for cracked reinforced concrete. Journal of Structural Engineering, 117(3): 715-732. https://doi.org/10.1061/(ASCE)0733-9445(1991)117:3(715)